Taylor-Couette flow with mixed convection heat transfer and variable properties in a horizontal annular pipe

Ismahane Chaieb, Toufik Boufendi, Xavier Nicolas

TAYLOR-COUETTE FLOW WITH MIXED CONVECTION HEAT TRANSFER AND VARIABLE PROPERTIES IN A HORIZONTAL ANNULAR PIPE

by

Ismahane CHAIEB [a], ***Toufik BOUFENDI*** [a*], ***and Xavier NICOLAS*** [b]

[a] Laboratory of Energy Physics, Department of Physics, Faculty of Exact Sciences, University Freres-Mentouri Constantine 1, Constantine, Algeria
[b] MSME, University Gustave Eiffel, CNRS UMR 8208, University Paris Est Creteil, Marne-la-Vallee, France

Original scientific paper
https://doi.org/10.2298/TSCI210218271C

Taylor-Couette flows in a horizontal annular gap between finite coaxial cylinders in rotor-stator configuration are numerically investigated. The inner cylinder (rotor) rotates at a constant angular velocity while the outer cylinder (stator) is at rest. They are limited at their extremities by two fixed walls that prevent axial fluid-flow. In addition, a heat transfer is generated by an imposed temperature difference, with the rotor hotter than the stator while the end-walls are adiabatic. The fluid physical properties are temperature dependent. This non-linear physics problem, with a strong coupling of the conservation equations and boundary conditions, is solved by a finite volume method with numerical schemes of second order space and time accuracies. The radius and aspect ratios and the Taylor, Grashof, and Prandtl numbers are the control parameters. The developed numerical code has been tested for different meshes and perfectly validated. Extensive calculations have been made in large ranges of the Taylor and Grashof numbers to analyze the Taylor-Couette flow in convection modes. The results highlight the dynamic and thermal instabilities generated in the Taylor-Couette flow from the appearance of Ekman cells to the Taylor vortex propagation in the entire annulus. The combined effect of these vortices with the secondary flow improves the heat transfer. Furthermore, the influence of the physical properties in the radial direction is more marked in the vicinity of the walls. Finally, we propose an empirical correlation of the Nusselt number in the studied parameter ranges.

Key words*: horizontal annular gap, vortex, mixed convection, variable properties, numerical simulation, Taylor-Couette flow*

Introduction

Because of their great importance for many engineering applications (*e.g.* electrical engines) and for the fundamental research, the study of heated rotary flows is still relevant. Inevitably, the heated Taylor-Couette flow (TCF) is the cornerstone for understanding this complex flow and heat transfer configuration. Since the Couette [1] and Taylor [2] precursor works, the topics of the rotating flows and the centrifugal instabilities resulting from it have been the subject of intense research activity. As a reminder, a TCF is that of a viscous fluid enclosed between two coaxial cylinders whose the inner cylinder rotates about its axis while the outer one

* Corresponding author, e-mail: tboufendi@umc.edu.dz

is fixed. The Taylor-Couette instability is a secondary flow formed by contra rotating toroidal vortices. It is induced by the force imbalance between the centrifugal force and the pressure gradient in the radial direction within the gap of the cylinders. It is possible to discern TCF with and without heat transfer. For the latter, an abundant bibliography highlights the influence of the increase of the Taylor number (rotational Reynolds number) as well as the appearance and evolution of the Taylor vortices in the gap, [3-6]. A mapping of the different states of the flow and successive instabilities ranging from steady-state Couette flow, abbreviated by circular Couette flow (CCF) until the turbulent Taylor flows has been developed by Andereck *et al*. [7] where each passage between two successive states is characterized by a critical Reynolds number [5]. Dutcher and Muller [8] have developed analytic formula for the determination of the critical Reynolds number for the newtonian Taylor-Couette primary instabilities for wide ranges of radius and aspect ratios. They showed that well-chosen dimensionless length scales can be used to fully describe the dependence of the critical conditions on the radius ratio.

For the second class of TCF with heat transfer, the studies are more recent and interesting bibliographic reviews [9-11] retrace the research evolution and propose open axes to explore. In addition the inertial and centrifugal forces, the buoyancy forces generated by temperature gradients must be taken into account. These forces are at the origin of a secondary flow in mixed convection and have been shown to improve heat transfer in horizontal ducts [12, 13]. For rotating flows, their influence in mixed convection mode is developed by Lei and Bakhtier [14] and Choi and Kim [15]. In their first experimental work, Bouafia *et al.* [16] carried out comparisons between two *smooth* and *grooved axially* configurations with and without axial flow. They show that the *smooth* configuration is more interesting in terms of heat exchange because the thermal heat transfer coefficient increases by 19%. Empirical correlations have also been proposed in [16]. The temperature gradient effect on centrifugal instabilities in a TCF between two vertical cylinders ($\eta = 0.8$ and $\Gamma = 114$), was experimentally studied by Lepiller *et al.* [17]. By imposing the Grashof number and varying the Taylor number, they show that, beyond a critical value of the Taylor number, a spiral pattern occurs giving rise to a finite extent propagating pattern. The numerical results from a linear stability analysis made by Mutabazi *et al.* [18] are in agreement with those of [17]. Sommerer and Lauriat [19] numerically studied the forced convection flows of an incompressible Newtonian fluid (air) in a grooved annular space, closed by fixed and adiabatic lateral rings. The inner cylinder, in rotation, is brought to a uniform temperature greater than that of the fixed outer cylinder which is grooved axially. As in [16], they found that heat transfer is lower than the one obtained in smooth geometries and propose very precise correlations linking the Nusselt number to the friction coefficient for a low rotation speed.

This work is a new contribution a better knowledge of the rotating flows. To the authors' knowledge on the basis of the visited documentation, the vertical configuration is more studied than the horizontal one and only the thermal variations in density are taken into account. The thermo-dependence of the other fluid physical properties can have a significant influence when a strong temperature gradient is present within the annular gap, especially when the fluid is simultaneously subjected to rotation and thermal convection in the gap: there will be a direct impact on the appearance and growth of the instabilities. Thus the purpose of the present analysis is to study TCF with heat transfer and temperature dependent physical properties in a horizontal annular pipe by numerical simulations.

Mathematical model

The geometry of the studied system is illustrated in fig. 1. It is an annular tube formed by two coaxial horizontal cylinders of the same length, L, and inner and outer radii R_i and

R_o, respectively, whose ends are closed by two fixed walls. The heated inner cylinder rotates at a constant angular velocity, Ω_i and R_i while the colder outer cylinder is at rest. The gap is filled with water whose temperature dependence of the dynamic viscosity and thermal conductivity is taken into account. Such a geometry is defined by the following set of parameters: the gap size, D_h, the ratio of radii, η, and the aspect ratio, Γ, respectively defined by:

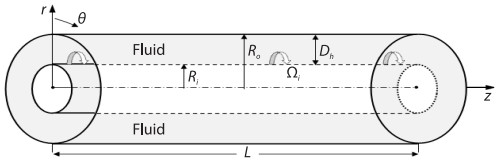

Figure 1. Geometry of the model

$$D_h = 2(R_o - R_i),\ \eta = R_o/R_i, \text{ and } \Gamma = L/D_h$$

The TCF with heat transfer and the temperature dependent physical properties of water are modeled by the mass, momentum and energy conservation equations, in a 3-D cylindrical co-ordinate system, with the appropriate initial and boundary conditions:

At $t = 0$:

$$\boldsymbol{V} = 0 \text{ and } T = 0 \tag{1}$$

At $t > 0$, using a bold notation for the vectorial form with a gravitational force oriented downward:

– Mass conservation equation

$$\frac{\partial \rho}{\partial t} + \nabla(\rho \boldsymbol{V}) = 0 \tag{2}$$

– Momentum equation

$$\frac{\partial(\rho \boldsymbol{V})}{\partial t} + \nabla(\rho \boldsymbol{V} \otimes \boldsymbol{V}) = -\nabla P + \nabla\left\{\mu(T)\left[\nabla \boldsymbol{V} + (\nabla \boldsymbol{V})^t\right]\right\} + \boldsymbol{F_g}(T) \tag{3}$$

– Energy equation

$$\frac{\partial(\rho C_p T)}{\partial t} + \nabla(\rho C_p T \boldsymbol{V}) = \nabla\left[k(T)\nabla T\right] \tag{4}$$

The rotational fluid movement is characterized either by the rotating Reynolds number or Taylor number defined by:

$$\mathrm{Re}_0 = \frac{R_i \Omega_i D_h}{\nu_0} \text{ and } \mathrm{Ta}_0 = 2\mathrm{Re}_0^2\left(\frac{1-\eta}{1+\eta}\right)$$

Boundary conditions

At $r^* = R_i^*$, $0 \le z^* \le L^*$, $0 \le \theta \le 2\pi$:

$$\boldsymbol{V_r^*} = \boldsymbol{V_z^*} = 0,\ \boldsymbol{V_\theta^*} = 1,\ T = T_i^* \tag{5}$$

At $r^* = R_o^*$, $0 \le z^* \le L^*$, $0 \le \theta \le 2\pi$:

$$\boldsymbol{V_r^*} = \boldsymbol{V_z^*} = \boldsymbol{V_\theta^*} = 0,\ T = T_o^* \text{ with } \left(T_i^* > T_o^*\right) \tag{6}$$

At $z^* = 0$ and L^*, $R_i^* \le r^* \le R_o^*$, $0 \le \theta \le 2\pi$:

$$\boldsymbol{V_r^*} = \boldsymbol{V_\theta^*} = \mathbf{V}_z^* = \frac{\partial T^*}{\partial z^*} = 0 \tag{7}$$

The thermodependence of the dynamic viscosity and thermal conductivity of water is obtained by smooth fitting of the tabulated values in Baehr and Stephan's book [20] and expressed by the dimensionless relationships:

$$\mu^*\left(T^*\right) = 0.23087 + 0.78727\exp\left(-\frac{T^*}{0.11386}\right) \tag{8}$$

$$k^*\left(T^*\right) = 1.00111 + 0.80477T^* - 1.06002T^{*2} \tag{9}$$

Nusselt numbers

The local heat transfer is quantified by the local Nusselt number defined:

$$\mathrm{Nu}\left(\theta, z^*\right) = \frac{h\left(\theta, z^*\right)D_\mathrm{h}}{k_0} = \frac{\left(\frac{k^*\partial T^*}{\partial r^*}\right)\Big|_{R_i^*}}{\left[T^*\left(R_i^*, \theta, z^*\right) - T_m^*\left(z^*\right)\right]} \tag{10}$$

where the dimensionless bulk fluid temperature is expressed:

$$T_m^*\left(z^*\right) = \frac{\int_{R_\mathrm{i}^*}^{R_\mathrm{o}^*}\int_0^{2\pi} V^*\left(r^*, \theta, z^*\right)T^*\left(r^*, \theta, z^*\right)r^*\,\mathrm{d}r^*\,\mathrm{d}\theta}{\int_{R_\mathrm{i}^*}^{R_\mathrm{o}^*}\int_0^{2\pi} V^*\left(r^*, \theta, z^*\right)r^*\,\mathrm{d}r^*\,\mathrm{d}\theta} \tag{11}$$

The axial Nusselt number Nu(z^*) is defined

$$\mathrm{Nu}\left(z^*\right) = \frac{1}{2\pi}\int_0^{2\pi}\mathrm{Nu}\left(\theta, z^*\right)\mathrm{d}\theta \tag{12}$$

Numerical method

The finite volume method [21] was used to discretize the conservation equations eqs. (1)-(4), in cylindrical co-ordinates, with the boundary conditions eqs. (5)-(7). Second order discretization schemes are used: the non-linear convective terms are discretized by the Adams-Bashforth scheme while the diffusive terms are discretized by the totally implicit central difference scheme. The velocity-pressure coupling is dealt with SIMPLER algorithm [21] with the time step $\Delta t = 75 \cdot 10^{-5}$. The obtained systems of algebraic equations are solved iteratively by the alternating direction implicit method based on Thomas algorithm. In order to ensure accurate and mesh independent solutions, the grid influence has been studied, especially in the axial direction. Thus the following grid sizes have been tested in the directions r^*, z^*, and θ, respectively: (26 × 142 × 45), (26 × 162 × 45), and (26 × 182 × 45), keeping the same radius ratio η = 0.767 and aspect ratio Γ = 37.36. As illustrated in fig. 2, the axial evolution of the azimuthal Nusselt number and the radial evolution of the temperature and angular component of the velocity in the annular gap are almost identical for the two finest grids. We therefore, chose to represent the results with the (26 × 162 × 45) grid.

The validation of our numerical code was done by comparing our results with those previously published. We first started with a comparison the analytical solution of the laminar incompressible and axisymmetric CCF given by [3, 9]:

$$V_\theta(r) = C_1 r + \frac{C_2}{r} \tag{13}$$

where the constants C_1 and C_2, for the case of a rotor-stator configuration, are:

$$C_1 = \frac{-\omega_i \eta^2}{1-\eta^2} \text{ and } C_2 = \frac{\omega_i R_i^2}{1-\eta^2}$$

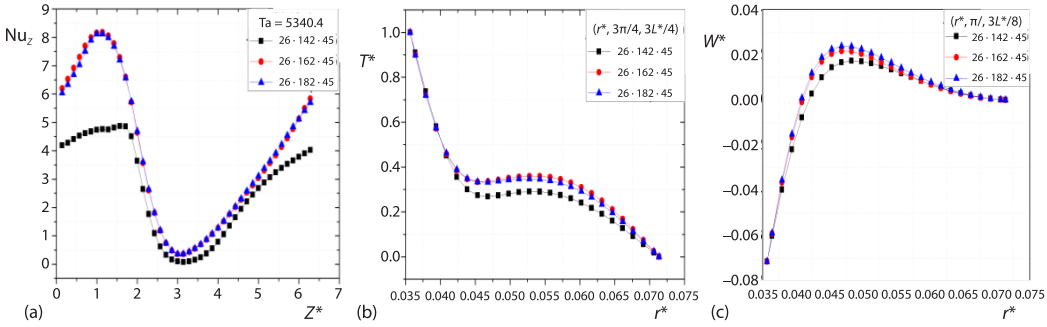

Figure 2. Mesh effects on: (a) the Nusselt number axial evolution, (b) the local temperature radial evolution at ($\theta = \pi/4$, $z^* = 3L^*/4$), (c) the local angular velocity radial evolution at ($\theta = \pi$, $z^* = 3L^*/8$), for aspect ratio $\Gamma = 37.36$, and Ta = 5340.4

The two solutions, analytical and numerical, are shown in fig. 3(a), for different values of the radius ratio, η. The following parameters, used in the work by Ait Moussa *et al*. [22], have been adopted for our numerical computations: Re = 56.25, R_i = 2.67 mm, and Γ = 23.35. We can see that there is a good agreement. In a second step, we considered the numerical results of [14] in the case of cellular flows in forced convection. Figure 3(b) shows the axial variation of the three velocity components at Re = 100, Gr = 0, and Γ = 6, at a middle radial position and at any point along the angular direction. The comparison shows a good agreement of our results with those of [14]. Finally, we proceeded to a last validation of our results with the experimental linear stability analysis carried out in [16] for TCF, for the geometric conditions summarized in tab. 1, with air as the working fluid and an imposed differential temperature gradient between the rotor (200 °C) and the stator (100 °C). In our simulations, the transition threshold between

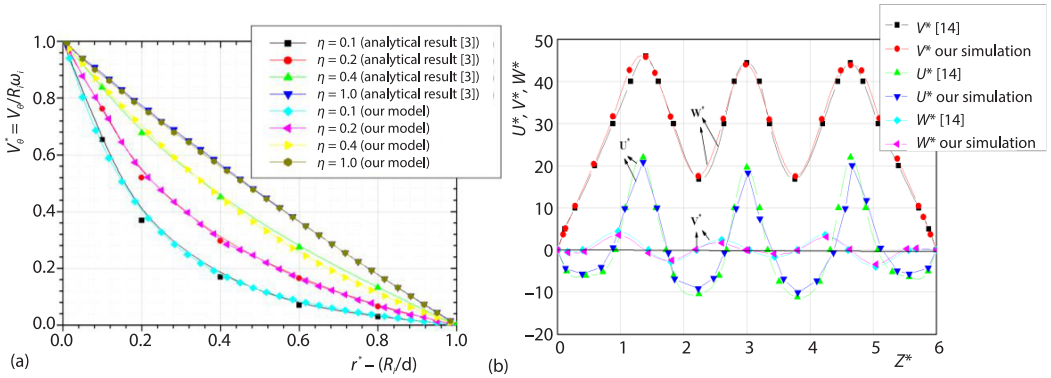

Figure 3. (a) Radial distribution of the velocity for the CCF in rotor-stator configuration for different radius ratios; present numerical results and analytical results of [3, 4] and (b) comparison of the calculated axial distribution of the three velocity components, at the middle radial position of the annular gap and at any arbitrary angular location with the results of [14]

the laminar parallel basic flow and the vortex laminar regime has been obtained for a critical Taylor number equal to $Ta_c = 1777.5$ and $Re_c = 75$. This is in good agreement with the critical thresholds obtained in [16] since they are equal to $Ta_{c1} = 1750$ and $Re_{c1} = 74.417$, respectively, with small differences equal to 1.6% for Ta_{c1} and 0.8% for Re_{c1}. We also obtain a clear similarity of the development of the isotherms in the annular gap between the two studies (not shown here).

Table 1. Geometric parameters used by [16]

Model	R_i [mm]	R_o [mm]	e [mm]	L [mm]	$\eta = R_i/R_o$	$\Gamma = L/e$
Smooth water gap	45.72	62.85	17.13	640	0.727	37.36

Results and discussion

All the results presented in this paper have been obtained for a moderately wide gap duct with the geometric characteristics given in tab. 1. The Prandtl number at the reference temperature is $Pr_0 = 8.082$ (distilled water). The Taylor and Grashof numbers, considered as operating parameters, varies in the range $505.6 \leq Ta \leq 2559.6$ and $10^3 \leq Gr \leq 10^4$. Particular attention is given to the combination of these intervals so as not to depart from the forced and mixed laminar convection domains. In the present study, the Richardson number ($Ri = Gr/Re^2$) measures the relative importance of the interaction between the buoyancy and rotational effects. It varies in the following range: $0 \leq Ri \leq 6.25$. One of the objectives of this study is to identify the different states of the flow and the critical thresholds for their appearance.

Velocity field and transverse flow

For the first case, fig. 4(a) (Ta = 505.6), the movement of the fluid in the majority of the gap, except close to the annular end-walls, is stable and follows the laminar regime called *Azimuthal Laminar Flow*, as denoted in [8]. The flow is globally 1-D, function of r^*, with the viscous forces still predominant over the centrifugal forces. Fig. 4(a) also shows that the first disturbances that appear are the *Ekman cells* in the vicinity of the end-walls. They are mainly due to the immobility of the end-walls [8]. Their direction of rotation is opposite in the vicinity of the two end-walls ($z^* = 0$, L^*): the first, at $z^* = 0$, turns counterclockwise while for the second, at $z^* = L^*$, turns clockwise. Figures 4(b) and 4(c) represent a small elevation of the Taylor number, from Ta = 790-1137.6. For these cases, the viscous force no longer compensates the centrifugal dynamic force, except in the central part of the gap where the streamlines keep their perfect radial stratification and horizontality (in the vertical bottom

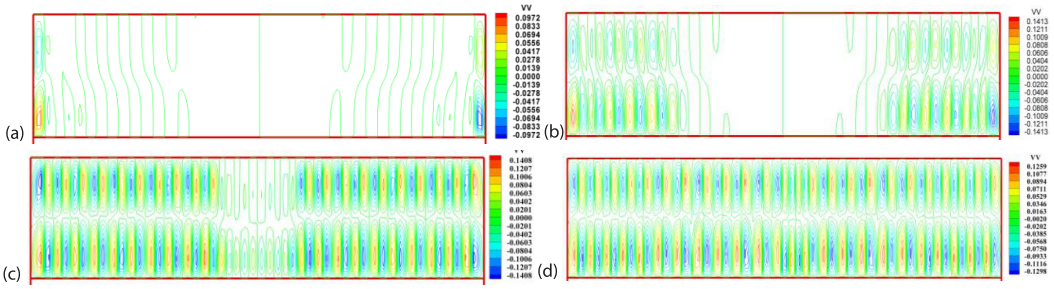

Figure 4. Isolines in the meridional plane (r^*, z^*) (vertical diametral plane), in the whole annular gap, for the various modes of instabilities for $505.6 \leq Ta \leq 2559.6$ and $Gr^* = 10^3$; (a) Ta = 505.6, (b) Ta = 790, (c) Ta = 1137.6, and (d) Ta = 2559.6

plane presented in figs. 4(b) and 4(c). This force imbalance, where the dynamic force is more important, generates toroidal vortices and induces the appearance of pairs of contrarotating cells of identical form. At this Taylor number magnitude, the axisymmetry is always preserved, with a perfect symmetrical arrangement of the cells in the axial direction, on either sides of the vertical diametric plane located in the middle of the duct. In fig. 4(c), the angular velocity is $-0.1408 \leq W^* \leq 0.1408$. By further increasing the angular velocity, a new bifurcation appears (after that mentioned in the validation section at 3) at a second critical value of the Taylor number equal to $Ta_{c2} = 2559.6$, see fig. 4(d). The dynamic force overcomes the viscous force in the whole annular gap: this state is called the Taylor vortex flow. The range of the angular velocity is $-0.1298 \leq W^* \leq 0.1259$. It should be noted that the value of Ta_{c2} can be different from one study to another, because it is very sensitive to the different parameters used [7]. In our case, this state is characterized by the formation of 24 pairs of juxtaposed and alterning counter-rotating cells, ie a total of 48 cells and 24 wavelengths formed over the entire length of the annular gap ($\Gamma = L^* = 37.36$). Accordingly the dimensionless size of a wavelength is equal to 1.56. The same dimensions and the perfect arrangement of the fluid cells between the two cylinders, symmetrically through the vertical median plane and the plane at $r^*/2$, deserves to be noted.

Figure 5 consolidates fig. 4 by presenting the formation of the contrarotating cells with isosurfaces of the angular velocity. One clearly distinguishes that the same angular speed iso-surface, equal to 0.124688, moves towards the outer cylindrical wall when the Taylor number increases.

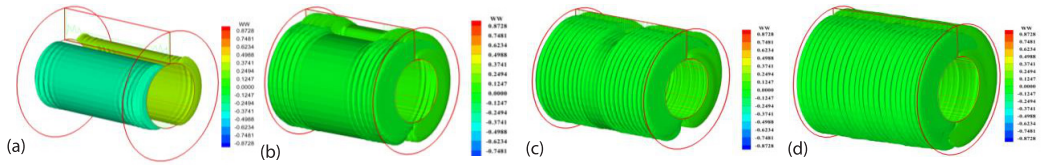

Figure 5. Same iso-angular velocity surface, equal to 0.124688, for different Taylor numbers $505.6 \leq Ta \leq 2559.6$ at $Gr = 10^3$; (a) Ta = 505.6, (b) Ta = 790, (c) Ta = 1137.6, and (d) Ta = 2159.6

Thermal field

To illustrate the development of the thermal field with the increase of the Taylor number, the isotherms are plotted in fig. 6, in a meridional plane (r^*, z^*) (of the annular gap (vertical plane at the bottom), for the four cases previously studied at $Gr = 10^3$. The corresponding Richardson numbers are equal to 0.625, 0.4, 0.28, and 0.12 indicating that the inertial forces are dominant over buoyancy forces. Despite the presence of a temperature gradient between the two cylinders, it remains too weak to be able to generate a natural-convection of the fluid in the gap. For the lowest Taylor number, fig. 6(a), the stratification of the isotherms with the thermal gradient in the radial direction is clearly visible in the central part of the gap, thus revealing the preponderance of a conductive heat transfer from the hot internal cylinder towards the cold external one. This distribution of isotherms is consistent with the variation of the conductive thermal gradient in ($1/r'$), which is found in annular geometries. Moreover, due to the existence of the Ekman cells in the vicinity of the end-walls which are adiabatic, a wavy character of the isotherm takes form, while respecting the orthogonality of the isotherms at the end-walls. As the Taylor number increases more, figs. 6(b) and 6(c), under the combined effect of the centrifugal and viscous forces which outweigh the buoyancy forces, the temperature gradient is always more important in the vicinity of the inner cylinder wall and it becomes weaker in the radial direction as one approaches the outer wall. The gradual propagation of the wave character in

the axial direction, initially generated by the Ekman cells, is still preserved. In fig. 6(d), at a higher Ta = 2559.6 but a smaller Ri = 0.12, the wavy isotherms occupy the whole gap, in the (r^*, z^*)-plane, due to their inertial transport. Thus, the results such as the velocity and temperature fields obtained at Gr = 10^3 are almost identical to those obtained at Gr = 0, corresponding to forced convection. The results that show the presence of natural-convection and, consequently, mixed convection flows are obtained at much higher Grashof/Richardson numbers, with Gr = $5 \cdot 10^3$ and 10^4 (or Ri = 1.02 and 1,23) for instance, as shown in figs. 7(c) and 7(d). With these values of Richardson number, natural-convection cells are generated by the buoyancy forces, that are no longer dominated by the forced convection caused by the centrifugal and viscous forces. Conversely, figs. 7(a) and 7(b) show circular isotherms and streamlines which follow a curvilinear path to join the movement of the inner cylinder. For these two cases, the symmetry with respect to a vertical diametral plane is respected and the preponderance of forced convection is confirmed. It can be seen that the center of the convection cell moves towards the top of the annular gap when Grashov or Richardson numbers increases.

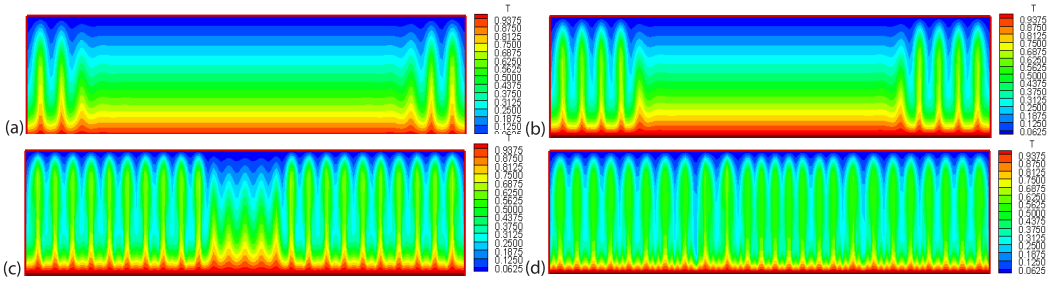

Figure 6. Thermal field in a longitudinal section (r^*, z^*) of the annular gap, for different Taylor numbers 505.6 ≤ Ta ≤ 2559.6 and Gr = 10^3; (a) Ta = 505.6 (Ri = 0.625), (b) Ta = 790 (Ri = 0.4), (c) Ta = 1137.6 (Ri = 0.28), and (d) Ta = 2559.6 (Ri = 0.12)

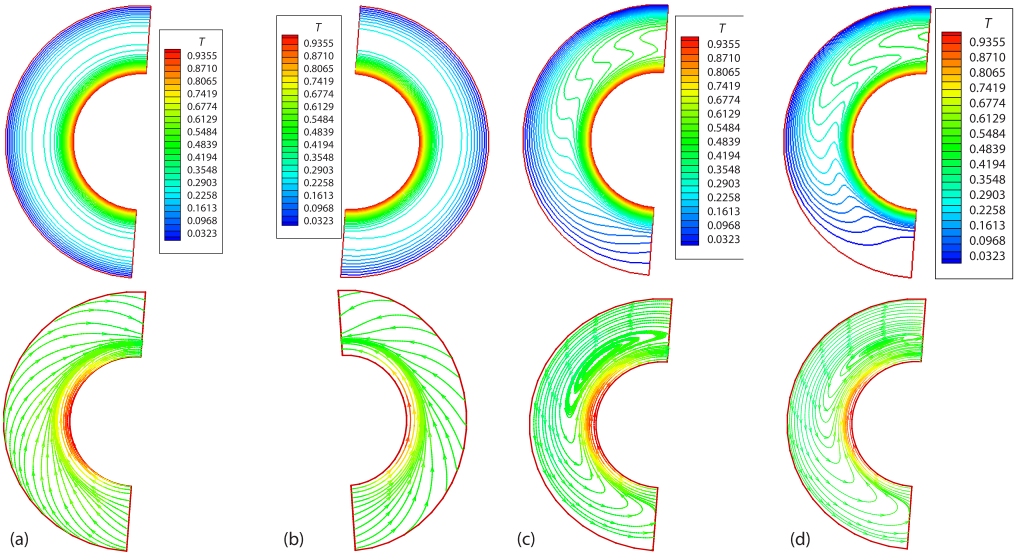

Figure 7. Isotherms and isolines with the increase of the Grashof number, at the same Taylor number, Ta = 2559.6 (Re = 90) and Ri = 0, 0.12, 1.02, and 1.23, in the half annular plane at z^* = 4.489; (a) Gr = 0, Ri = 0, (b) Gr = 10^3, Ri = 0.12, (c) Gr = $5 \cdot 10^3$, Ri = 1.02, and (d) Gr = 10^4, Ri = 1.23

Figures 8(a)-8(d) show the presence of a non-symmetrical secondary flow in the whole annular plane. It is created by the buoyancy forces at higher Richardson numbers (Ri = 1.23 and 6.25 or Re = 40, and 90 at Gr = 10^4). In both cases, we can clearly see the formation of two counter-rotating cells of different dimensions. The largest occupying 3/4 of the gap and moves counterclockwise, while the smaller is pushed towards the lower and right part of the gap and flows in a clockwise direction. In both cases, the centers of the vortices are located in the middle zone of the gap. This configuration with a strong transverse flow in (r, θ) plane modifies the axisymmetric distribution of the fluid temperature with the lowest fluid temperatures located in the lower part of the gap, see fig. 7.

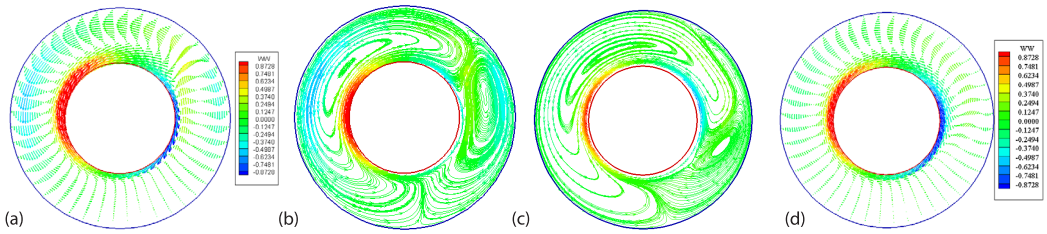

Figure 8. Velocity vectors and isolines of the secondary flow in (r^*, θ) plane at $z^* = 4.489$ for Gr = 10^4; (a) and (b) Re = 40, Ri = 6.25, (c) and (d) Re = 90, Ri = 1.23

Furthermore, the existence of a thin boundary-layer, with a thickness of the order of $4\Delta r^*$, can be noted very close to the inner cylinder which directly follows the rotational movement of the cylinder, in the clockwise direction. Beyond this thickness, due to the viscous driving force, a boundary-layer detachment phenomenon appears, due to the natural-convection effect which drives the fluid particles in a counterclockwise angular movement. In this work, we have considered that the physical properties of the fluid vary with temperature. It is then interesting to represent the variations of the thermal conductivity and dynamic viscosity in the radial direction of the gap for the parameters studied. Figure 9 illustrates these variations as a function of r^*. It clearly appears that, in the vicinity of the inner hotter cylinder, the conductivity increase with the temperature increase while the viscosity is the lowest. Close to the outer colder duct, the conductivity also decreases while the viscosity undergoes a marked increase. These behaviors are physically acceptable in accordance with eqs. (8) and (9). To quantify the wall-fluid heat transfer, the variations of the local Nusselt number on the inner cylinder are illustrated in fig. 10 for Gr = 10^3 and for the same Ta-values as in figs. 4 and 5, that is in forced convection regimes. The local Nusselt number is directly influenced by the temperature distribution which is itself related to the velocity field and the presence of the counter-rotating cells. It is weaker in the thermally stratified regime and shows a clear increase as the Taylor number increases. In quantitative terms, the maxima of Nusselt number goes from 6.033-17.8958 for Ta = 505.6-2559.6. In tab. 2, we present the mean Nusselt numbers of all the simulated cases at Gr = 10^3. In this forced convection regime, we found the following correlation of

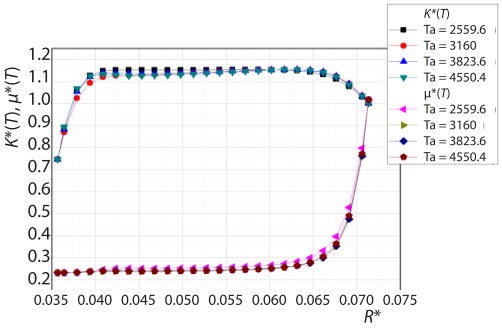

Figure 9. Thermal conductivity and dynamic viscosity variations in the radial direction of the gap for each Taylor number at Gr = 0

the averaged Nusselt number as a function of the Taylor number: $Nu_A = 0.0132Ta^{0.8228}$. It is important to specify that, in the domain of large Grashof numbers, ($5 \cdot 10^3$ or 10^4), for the same Grashof number, natural-convection can becomes negligible at small Taylor numbers while it becomes more important for larges Taylor numbers. That is to say, even though Grashof is large, the centrifugal and viscous forces can still annihilate natural-convection at low Taylor numbers. But, as the number of Taylor number increases, natural-convection progressively intensifies to counteract the retarding effects of the viscous forces. Therefore, for high Grashof number, the heat transfer is better at high Taylor number. Thus, for the geometric conditions of our model, we find that, for obtaining a better heat transfer, Taylor number must be greater than or equal to 1294.97 (Re = 64) for $Gr = 5 \cdot 10^3$, and for $Gr = 10^4$, Taylor number must be greater than or equal to Ta = 1778.35 (Re = 75).

Table 2. Average Nusselt numbers for $Gr = 10^3$

Ta	Nu_A
505.6	2.3302
790	2.7721
1137.6	4.4018
1548.4	6.1549
2022.4	7.0442
2559.6	7.8768

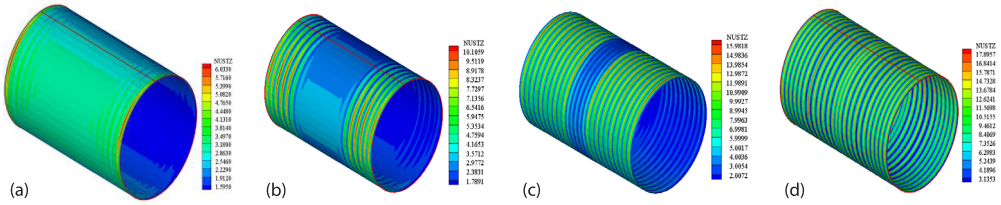

Figure 10. Evolution of the local Nusselt number for different Taylor number and $Gr = 10^3$; (a) Ta = 505.6, (b) Ta = 790, (c) Ta = 1137.6, and (d) Ta = 2559.6

Conclusion

This study concerns the 3-D numerical simulation of the TCF with convection heat transfer in a horizontal annular duct. The inner and hotter cylinder is driven by a constant rotation velocity while the outer and colder one is stationary. This is a rotor-stator system with fixed geometrical parameters and thermal dependent fluid properties. The operating parameters are the Taylor or rotational Reynolds numbers and the Grashof or Richardson numbers. Extensive results have been obtained to show the effect of the Taylor number ($505.6 \leq Ta \leq 2559.66$) on the dynamic and thermal fields in the gap, for Grashof number $10^3 \leq Gr \leq 10^4$. We obtain three laminar regimes: at low Taylor number, only Ekman cells are present; for a moderate augmentation of Taylor number, there is a propagation of contrarotative cells towards the center of the gap with vertical and horizontal symmetries; for high Taylor number, a complete occupation of the gap by the cells is observed with symmetry respect or not. The thermal and dynamic behaviors are similar. In term of heat transfer, at $Gr = 10^3$, the forced convection is the dominant mode while, increasing Grashof number to $5 \cdot 10^3$ to 10^4, intensifies the buoyancy forces that generate a secondary flow and, as a result, the mixed convection. At $Gr = 10^3$, heat transfer is improved as Taylor number is increased. But for high Grashof numbers, we conclude that the evolution of the local Nusselt number as a function of the Taylor number begins with a decay phase as long as the Taylor numbers are small, to reach a minimum, and finally initiate a monotonic growth with large Taylor numbers. Finally, in the range of Taylor number values explored, we propose the following empirical correlation of the Nusselt number in forced convection (Gr = 0) and for a very low natural-convection ($Gr = 10^3$): $Nu = 0.0132Ta^{0.8228}$.

Acknowledgment

The authors acknowledge the Energy Physics Laboratory of UFMC1 and the Algerian DGRSDT- MESRS for the financial support FNR. They also gratefully thank Dr. Touahri Sofiane, member of research team of Prof. Boufendi for his support in the numerical aspect of this paper.

Nomenclature

D_h – hydraulic diameter, [$= 2(R_o - R_i)$], [m]
Gr – Grashof number, ($= g\beta\Delta T D_h^5/k_0\nu_0$), [–]
g – gravitational acceleration, (= 9.81), [ms^{-2}]
k^* – dimensionless thermal conductivity, ($= k/k_0$), [–]
L^* – dimensionless annulus length, ($= L/D_h$), [–]
Nu(θ, z^*) – local Nusselt number [$= h(\theta, z)D_h/k_0$], [–]
P – pressure, [kgm^{-1}s^{-2}]
Pr – Prandtl number ($= \nu/\alpha$), [–]
Re – Reynolds number ($= R_i\Omega_i D_h/\nu_0$),[–]
Ri – Richardson number ($=$ Gr/Re^2) ,[–]
R_i, R_o – inner (rotor), outer (stator) radius, [m]
r^*, θ, z^* – dimensionless radial, angular and axial co-ordinate
T^* – dimensionless temperature [$= (T - T_o)/(T_i - T_o)$]
Ta – Taylor number, {$= 2\text{Re}^2[(1 - \eta)/(1 + \eta)]$}, [–]
T_i, T_o – inner (rotor), outer (stator) temperature, respectively, [°C]
T_0 – reference temperature, [°C]
t^* – dimensionless time ($= D_h/R_i\Omega_i$), [–]
$\mathbf{V}_r^*$, $\mathbf{V}_\theta^*$, $\mathbf{V}_z^*$ – dimensionless velocities components, ($= V_r/R_i\Omega_i$, $= V_\theta/R_i\Omega_i$, $= V_z/R_i\Omega_i$), [–]

Greek symbols

α – thermal diffusivity, [m^{2}s^{-1}]
β – thermal expansion coefficient,[°C^{-1}]
Γ – aspect ratio ($= L/D_h$), [–]
Δ – difference, [–]
η – ratio of radii ($= R_o/R_i$), [–]
θ – angular co-ordinate, [rad]
μ^* – non-dimensional dynamic viscosity ($= \mu/\mu_0$), [–]
ρ – density, [kgm^{-3}]
Ω – angular rotor velocity, [rads^{-1}]

References

[1] Couette, M., Study on the Friction of Liquids, *Chim. Phys*, *21* (1890), pp. 433-510
[2] Taylor, G. I., Stability of a Viscous Liquid Contained between Two Rotating Cylinders, *Philosophical Transaction*, *223* (1923), 8, pp. 289-343
[3] Childs, P., R, N., *Rotating Flow*, Elsevier Science and Technology Rights, Burlington, Vt., USA, 2011
[4] Hopfinger, E. J., *Rotating Fluids in Geophysical and Industrial Applications*, Springer, Paris, France, 1992
[5] Di-Prima, R. C., Swinney, H. L., Instabilities and Transition in Flow between Concentric Cylinders, in: *Topics in Applied Physics*, *Hydrodynamic Instabilities and the Transition Turbulence*, (Eds. H. L. Swinney, Gollub J. P., Springer-Verlag, 1981, Vol. 34, pp. 139-180
[6] Vedantam, S., Joshi, J. B., Annular Centrifugal Contactors – A Review, *Chemical Engineering Research and Design*, *84* (2006), 7, pp. 522-542
[7] Andereck, C. D., *et al*., Flow Regimes in a Circular Couette System with Independently Rotating Cylinders, *Journal of Fluid Mech*, *164* (1986), Mar., pp. 155-183
[8] Dutcher, C. S., Muller, S. J., Explicit Analytic Formulas for Newtonian Taylor-Couette Primary Instabilities, *Physical Review E*, *75* (2007), Apr., pp. 47301-47305
[9] Maron, D., M., Cohen, S., Hydrodynamics and Heat/Mass Transfer Near Rotating Surfaces, *Advances in Heat Transfer*, *21* (1991), Dec., pp. 141-183
[10] Childs, P., R., Long, C., A., A Review of Forced Convective Heat Transfer in Stationary and Rotating Annuli, Proc. of the Inst. of Mech. Eng., Part C: *Journal Mech. Eng. Science*, *210* (1996), 23, pp. 123-134
[11] Fenot, M., *et al*., A Review of Heat Transfer between Concentric Rotating Cylinders with or without Axial Flow, *International Journal of Thermal Sciences*, *50* (2011),7, pp. 1138-1155
[12] Touahri, S., Boufendi, T., Conjugate Heat Transfer with Variable Fluid Properties in a Heated Horizontal Annulus, *Heat Transfer Research*, *46* (2015), 11, pp. 1019-1038
[13] Touahri, S., Boufendi, T., Numerical Study of the Conjugate Heat Transfer in a Horizontal Pipe Heated by Joulean Effect, *Thermal Sciences*, *16* (2012), 1, pp. 53-67
[14] Lei, Y., Bakhtier, F., The 3-D Mixed Convection Flows in a Horizontal Annulus with a Heated Rotating Inner Circular Cylinder, *Int. J. Heat and Mass Transfer*, *35* (1992), 8, pp.1947-1956

[15] Choi, J. Y., Kim, M., U., The 3-D Linear Stability of Mixed Convective Flow between Rotating Horizontal Concentric Cylinders, *Int. J. Heat and Mass Transfer*, *38* (1995), 2, pp. 27-285
[16] Bouafia, M., *et al.*, Experimental Analysis of Heat Transfer in Narrow and Grooved Annular Space with Rotating Inner Cylinder (in french), *Int. J. Heat and Mass Transfer*, *41* (1998), 10, pp. 1279-1291
[17] Lepiller, V., *et al*., Hydrothermal Instabilities in a Vertical Cylindrical Annular Subjected to a Strong Radial Temperature Gradient, *Proceedings*, 18th French Congress of Mechanics, Grenoble, France, 2009
[18] Mutabazi, I., *et al*., Flow Instabilities in a Vertical Differentially Rotating Cylindrical Annulus with a Radial Temperature Gradient, *EUROMECH Colloquium*, *525* (2011), June, pp. 21-23
[19] Sommerer, Y., Lauriat, G., Numerical Study of Steady Forced Convection in a Grooved Annulus Using a Design of Experiments, *Journal of Heat Transfer*, *123* (2001), 5, pp. 837-847
[20] Baehr, H. D., Stephan, K., *Heat and Mass Transfer*, Springer-Verlag, Berlin, Germany, 1998
[21] Patankar, S. V., *Numerical Heat Transfer and Fluid-Flow*, McGraw Hill, New York, USA, 1980
[22] Ait-Moussa, *et al*., Numerical Simulations of Co-and Counter-Taylor-Couette Flows: Influence of the Cavity Radius Ratio on the Appearance of Taylor Vortices, *American Journal of Fluid Dynamics, 5* (2015), 1, pp. 17-22

Paper submitted: February 18, 2021
Paper revised: August 25, 2021
Paper accepted: September 1, 2021